1 Introduction

For over 20 years the SPICE Gummel-Poon (SGP) model (Gummel, 1970; Nagel, 1975) has been the IC industry standard for circuit simulation for bipolar junction transistors (BJTs). This is a testament to the sound physical basis of the model. However, the SGP model is not perfect. Some of the shortcomings of the SGP model have been known for a long time, such as its inability to model collector resistance modulation (quasi-saturation) and parasitic substrate transistor action. And the inexorable advance of IC manufacturing technologies has magnified the inaccuracies in other aspects of the SGP model, e.g. the Early effect formulation for modeling output conductance g_o. The approximations that underlie the SGP Early effect model (Nagel, 1975; McAndrew, 1996) were reasonable for modeling wide base BJTs (see Figure 1), but are not reasonable for modeling narrow base BJTs (see Figure 2). And as Figure 2 shows, a significant portion of the capacitances of a double poly BJT are from fixed (i.e. bias independent) dielectric capacitances, which are not included in the SGP model.

Improved BJT models have been presented (Turgeon, 1980; Kull, 1985; de Graaff, 1985; Stubing, 1987; Jeong, 1989), however none have become an industry standard to replace the SGP model. VBIC (which stands for the Vertical Bipolar Inter-Company model) was defined by a group of representatives from the IC and CAD industries to try to rectify this situation. VBIC is public domain, and complete source code is publicly available. VBIC is also as similar as possible to the SGP model, to leverage the existing knowledge and training of characterization and IC design engineers.

The following are the main modeling enhancements of VBIC over SGP:

- improved Early effect (g_o) modeling
- quasi-saturation modeling
- parasitic substrate transistor modeling
- parasitic fixed (oxide) capacitance modeling
- avalanche multiplication modeling
- improved temperature dependence modeling
- decoupling of base and collector currents
- electrothermal (self heating) modeling
- C_∞ continuous (smooth) modeling
- improved heterojunction bipolar transistor (HBT) modeling.

The additional capabilities of VBIC are turned off with the default values of its model parameters, so VBIC defaults to being close to the SGP model, the exception being the Early effect formulation which is different between the two models.

The presentation and examples used here are mostly for 4-terminal vertical NPN transistors, Figures 1 and 2 show typical structures that VBIC is intended to model. VBIC can also be used for vertical PNP modeling, and for HBT modeling, but it is not directly targeted at lateral BJT modeling. Vertical PNPs in smartpower technologies are often 5-terminal devices, and VBIC can be used in a subcircuit to model such devices, however this does not properly model transistor action of the second parasitic BJT.

Compact models for circuit simulation should scale properly with device geometry. However, for BJTs the plethora of layout topologies and structure make this impossible to do in a comprehensive manner. Therefore VBIC explicitly does not include any geometry mappings. It is assumed that geometry scaling for VBIC will be handled either in pre-processing for the generation of model libraries for circuit simulation, or via scaling relations specific to a particular technology implemented either in the simulator or the CAD system used for design.

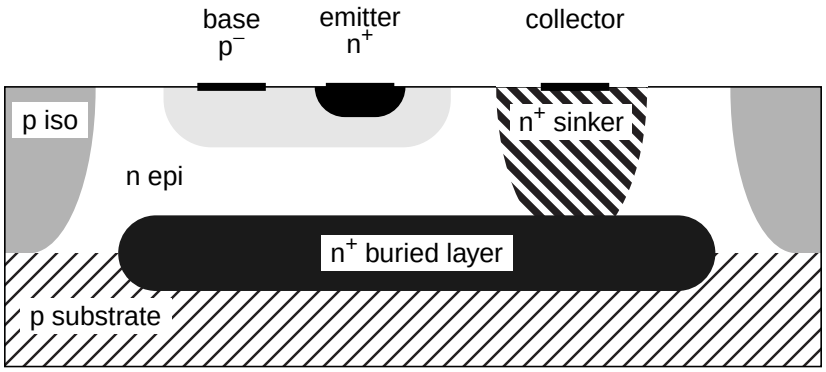

Figure 1 Junction isolated diffused NPN structure.

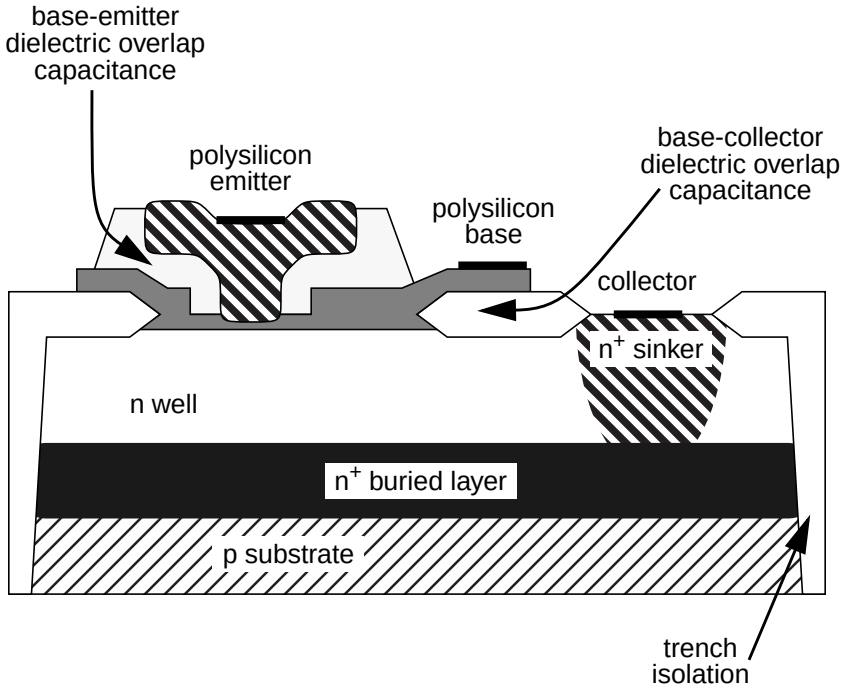

Figure 2 Trench isolated double poly NPN structure.

2 VBIC Equivalent Network

Figure 3 shows the equivalent network of VBIC, which includes an intrinsic NPN transistor, a parasitic PNP transistor, parasitic resistances and capacitances, a local thermal network (used only with the electrothermal version of the model), and a circuit that implements excess phase for the forward transport current $\mathrm{I}_{\mathrm{tzf}}$.

For the electrothermal version of VBIC the branch currents and charges in the electrical part of the model also depend on the local temperature rise, the voltage on the node `dt`. The thermal

equivalent circuit includes two nodes external to the model so that the local heating and dissipation can be connected to a thermal network that models the thermal properties of the material in which the BJT and surrounding devices are built.

Although the equivalent network of Figure 3 is drawn with resistances (fixed and bias dependent), capacitances, and current sources, the elements should generally be considered as voltage controlled current sources $I(V_1, V_2, \ldots V_3)$ and voltage controlled charge sources $Q(V_1, V_2, \ldots V_3)$. Simple resistors and capacitors are then current and charge sources, respectively, controlled only by the voltage across them. Branch currents and charges that are controlled by more than one branch voltage, e.g. R_{BI}/q_b and Q_{be}, include trans-conductance and trans-capacitance elements when they are linearized, as is required for DC solution and for AC, noise and transient simulations.

Table 1 lists each of the elements of the VBIC equivalent network of Figure 3, with a short description of the function of the element.

Name	**Element**
I_{tzf}	forward transport current, zero phase
I_{txf}	forward transport current, with excess phase
Q_{cxf}, F_{lxf}	excess phase circuit capacitance and inductance
I_{tzr}	reverse transport current, zero phase
I_{be}	intrinsic base-emitter current
I_{bex}	extrinsic (side) base-emitter current
Q_{be}	intrinsic base-emitter charge (depletion and diffusion)
Q_{bex}	extrinsic (side) base-emitter charge (depletion only)
I_{bc}	intrinsic base-collector current
I_{gc}	base-collector weak avalanche current
Q_{bc}	intrinsic base-collector charge (depletion and diffusion)
Q_{bcx}	extrinsic base-collector charge (diffusion only)
I_{tfp}	parasitic forward transport current
I_{trp}	parasitic reverse transport current
I_{bep}	parasitic base-emitter current
Q_{bep}	parasitic base-emitter charge (depletion and diffusion)
I_{bcp}	parasitic base-collector current
Q_{bcp}	parasitic base-collector charge (depletion only)
R_{CX}	extrinsic collector resistance (fixed)
R_{CI}	intrinsic collector resistance (modulated)

Table 1 Elements of VBIC equivalent network

Name	Element
R_{BX}	extrinsic base resistance (fixed)
R_{BI}/q_b	intrinsic base resistance (modulated)
R_E	emitter resistance (fixed)
R_{BIP}/q_{bp}	parasitic base resistance (modulated)
R_S	substrate resistance (fixed)
C_{BEO}	parasitic base-emitter overlap capacitance (fixed)
C_{BCO}	parasitic base-collector overlap capacitance (fixed)
I_{th}	thermal (heat generation) source
R_{TH}, C_{TH}	thermal resistance and capacitance (fixed)

Table 1 Elements of VBIC equivalent network

3 VBIC Model Formulation

The core of VBIC, as with most BJT models, is the transport (collector) current model, which follows directly from Gummel (1970). For electrons, the continuity equation is

$$\nabla \bullet \mathbf{J}_e = q\left(\frac{\partial n}{\partial t} + R_e - G_e\right) \tag{1}$$

where $\mathbf{J}_e$ is the electron current density, q is the magnitude of the electronic charge, n is the mobile electron concentration, and R_e and G_e are the electron recombination and generation rates, respectively. The drift-diffusion relation for electrons is

$$\mathbf{J}_e = \mu_e(kT\nabla n - qn\nabla\psi) = -q\mu_e n\nabla\phi_e \tag{2}$$

where μ_e is the electron mobility, k is Boltzmann's constant, T is the temperature in degrees Kelvin, ψ is the electrostatic potential, and ϕ_e is the electron quasi-Fermi potential. The mobile electron concentration is

$$n = n_{ie}\exp\left(\frac{\psi - \phi_e}{V_{tv}}\right) \tag{3}$$

where n_{ie} is the effective intrinsic concentration, including bandgap narrowing, and $V_{tv} = kT/q$ is the thermal voltage.

$$p = n_{ie}\exp\left(\frac{\phi_h - \psi}{V_{tv}}\right) \tag{4}$$

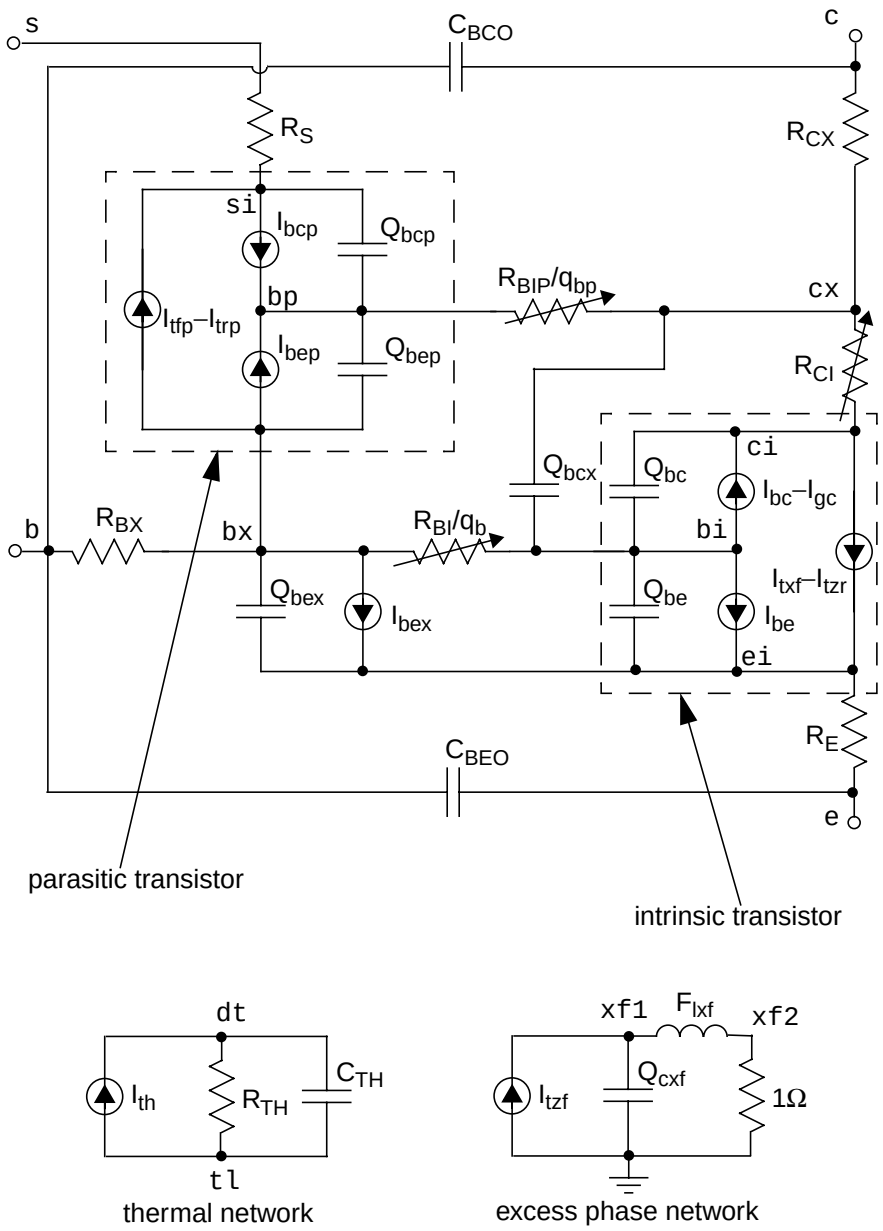

Figure 3 VBIC equivalent network.

gives the mobile hole concentration, where ϕ_h is the hole quasi-Fermi potential.

Figure 4 shows a representative 1-dimensional doping profile of a vertical NPN, through the region of the device under the emitter where bipolar transistor action occurs.

Analysis of the transport in the base region of a BJT is based on equations (1) and (2). In the steady state in the x dimension only, ignoring recombination and generation (which is generally reasonable for the base of a BJT), gives

$$\frac{\partial J_{ex}}{\partial x} = 0 \tag{5}$$

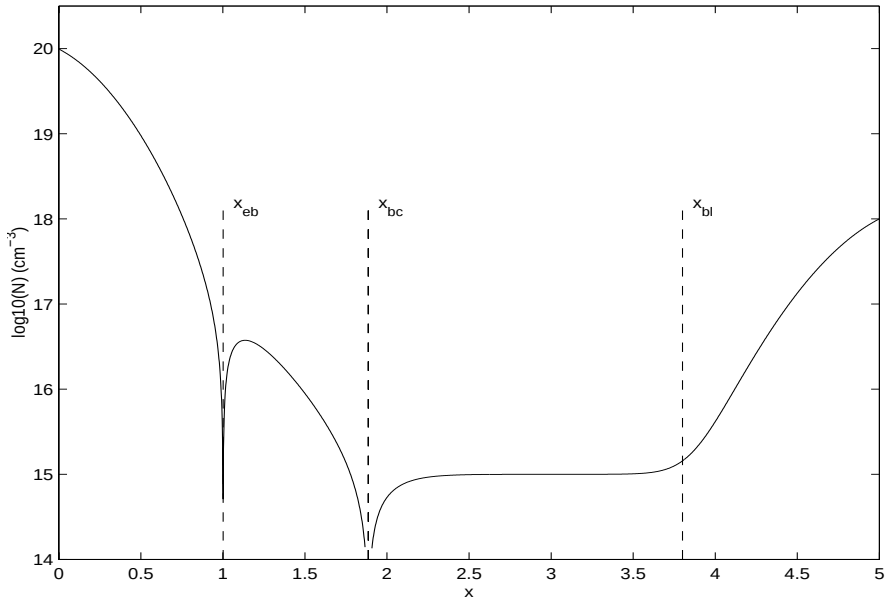

Figure 4 1-dimensional doping profile.

directly from equation (1), and

$$J_{ex} = \text{constant} = -q\mu_e n\frac{\partial\phi_e}{\partial x} = q\mu_e n_{ie} V_{tv}\exp\left(\frac{\psi}{V_{tv}}\right)\frac{\partial\exp(-\phi_e/V_{tv})}{\partial x} \tag{6}$$

follows after some manipulation. Integrating equation (6) from the emitter ($x = x_{eb}$, where $\phi_e = \phi_{ee}$) to the collector ($x = x_{bc}$, where $\phi_e = \phi_{ec}$) through the base gives

$$J_{ex} = qV_{tv}\frac{\exp(-\phi_{ec}/V_{tv}) - \exp(-\phi_{ee}/V_{tv})}{\int_{x_{eb}}^{x_{bc}}\frac{\exp(-\psi/V_{tv})}{\mu_e n_{ie}}dx} \tag{7}$$

where ψ, μ_e and n_{ie} are all functions of position x. Multiplying both the numerator and the denominator of equation (7) by $\exp(\phi_h/V_{tv})$, and noting that the difference between hole and electron quasi-Fermi potentials across a junction is just the voltage applied across the junction, gives

$$J_{ex} = qV_{tv}\frac{\exp(V_{bci}/V_{tv}) - \exp(V_{bei}/V_{tv})}{\int_{x_{be}}^{x_{bc}}\frac{p}{\mu_e n_{ie}^2}dx} \tag{8}$$

where $V_{bei} = \phi_h - \phi_{ee}$ is the intrinsic base-emitter voltage, between nodes `bi` and `ei` of the equivalent network of Figure 3, and $V_{bci} = \phi_h - \phi_{ec}$ is the intrinsic base-collector voltage, between nodes `bi` and `ci`. Equation (8) is the basis of Gummel-Poon type BJT models (Gummel 1970). It shows that the collector current varies exponentially with applied bias, and is controlled by the integrated base charge, which is commonly called the base Gummel number.

Note that the limits of integration through the base are not rigorously defined above. The analysis is valid across any region in which the hole quasi-Fermi level is constant. In practice, it is convenient to define the base region as where ϕ_h is constant.

Use of equation (8) in VBIC requires the base charge to be modeled as a function of applied bias. For VBIC the base charge is normalized with respect to its value at zero applied bias, and includes depletion and diffusion components (Gummel, 1970; Getreu, 1976). The VBIC (zero excess phase) forward and reverse transport currents are

$$I_{tzf} = I_S \frac{\exp(V_{bei}/(N_F V_{tv})) - 1}{q_b} \tag{9}$$

$$I_{tzr} = I_S \frac{\exp(V_{bci}/(N_R V_{tv})) - 1}{q_b} \tag{10}$$

where I_S is the transport saturation current, N_F and N_R are the forward and reverse ideality factors, and q_b is the normalized base charge. The ideality factors are introduced as parameters, rather being forced to be 1, to allow flexibility in modeling, to recognize that the theoretical analyses above are approximate, because non-ideal transport behavior is observed in HBTs, and for compatibility with the SGP model.

Consider a BJT operating in low level injection, in the forward active model so that $V_{bei} > 0$ and $V_{cei} = V_{bei} - V_{bci} > 0$. Considering only the transport current, and ignoring the Early effect, the power dissipated is

$$I_S\left(\exp\left(\frac{V_{bei}}{N_F V_{tv}}\right) - \exp\left(\frac{V_{bci}}{N_R V_{tv}}\right)\right)V_{cei} \quad . \tag{11}$$

$$= I_S \exp\left(\frac{V_{bei}}{N_F V_{tv}}\right)\left(1 - \exp\left(\frac{V_{bei}}{V_{tv}}\left(\frac{1}{N_R} - \frac{1}{N_F}\right)\right)\exp\left(-\frac{V_{cei}}{N_R V_{tv}}\right)\right)V_{cei}$$

For the power dissipation to be positive, which it must be physically, it follows that

$$\exp\left(\frac{V_{bei}}{V_{tv}}\left(\frac{1}{N_R} - \frac{1}{N_F}\right)\right)\exp\left(-\frac{V_{cei}}{N_R V_{tv}}\right) \le 1 \tag{12}$$

must hold. Given that V_{cei} can be arbitrarily close to zero, so that $\exp(-V_{cei}/(N_R V_{tv}))$ can be arbitrarily close to unity, equation (12) implies that

$$\frac{1}{N_R} - \frac{1}{N_F} \le 0 \tag{13}$$

and hence

$$N_F \le N_R \tag{14}$$

for the power dissipation to be positive. A similar analysis in the reverse active region of

operation shows that the power dissipation is

$$I_S \exp\left(\frac{V_{bci}}{N_R V_{tv}}\right)\left(1 - \exp\left(\frac{V_{bci}}{V_{tv}}\left(\frac{1}{N_F} - \frac{1}{N_R}\right)\right)\exp\left(-\frac{V_{eci}}{N_F V_{tv}}\right)\right)V_{eci} \tag{15}$$

and because $V_{bci} > 0$ and $V_{eci} = V_{bci} - V_{bei} > 0$ this implies that

$$N_R \le N_F . \tag{16}$$

Equations (14) and (16) mean that

$$N_R = N_F \tag{17}$$

must hold, for the model to be passive and not generate power. Although equation (17) was derived under some restrictive approximations, and data from HBTs clearly shows that $N_R \neq N_F$, it is apparent that with certain values of model parameters VBIC (and SGP) can be non-passive. It is undesirable for a model to rely on having certain values of model parameters to display reasonable behavior, a good model should always have reasonable behavior regardless of model parameter values. Therefore for silicon devices it is recommended that $N_R = N_F$ be maintained for VBIC.

The normalized base charge is

$$\begin{aligned} q_b &= q_1 + \frac{q_2}{q_b} \\ q_1 &= 1 + \frac{q_{je}}{V_{ER}} + \frac{q_{jc}}{V_{EF}} \\ q_2 &= \frac{I_S(\exp(V_{bei}/(N_F V_{tv})) - 1)}{I_{KF}} + \frac{I_S(\exp(V_{bci}/(N_R V_{tv})) - 1)}{I_{KR}} \end{aligned} \tag{18}$$

where V_{EF} and V_{ER} are the forward and reverse Early voltages, and I_{KF} and I_{KR} are the forward and reverse knee currents. The normalized depletion charges are

$$q_{je} = q_j(V_{bei}, P_E, M_E, F_C, A_{JE}),\ q_{jc} = q_j(V_{bci}, P_C, M_C, F_C, A_{JC}) \tag{19}$$

where P_E and P_C are the built-in potentials and M_E and M_C are the grading coefficients of the base-emitter and base-collector junctions, respectively. The normalized depletion charge function q_j is such that

$$c_j(V, P, M, F_C, A) = \frac{\partial q_j(V, P, M, F_C, A)}{\partial V} \approx \frac{1}{(1 - V/P)^M} \tag{20}$$

for reverse and low forward bias. If the depletion capacitance smoothing parameters A_{JE} and A_{JC} are less than zero c_j smoothly limits to its value at $F_C P$, otherwise c_j linearly increases for

$V > F_C P$ to match the SGP model, see Figure 5.

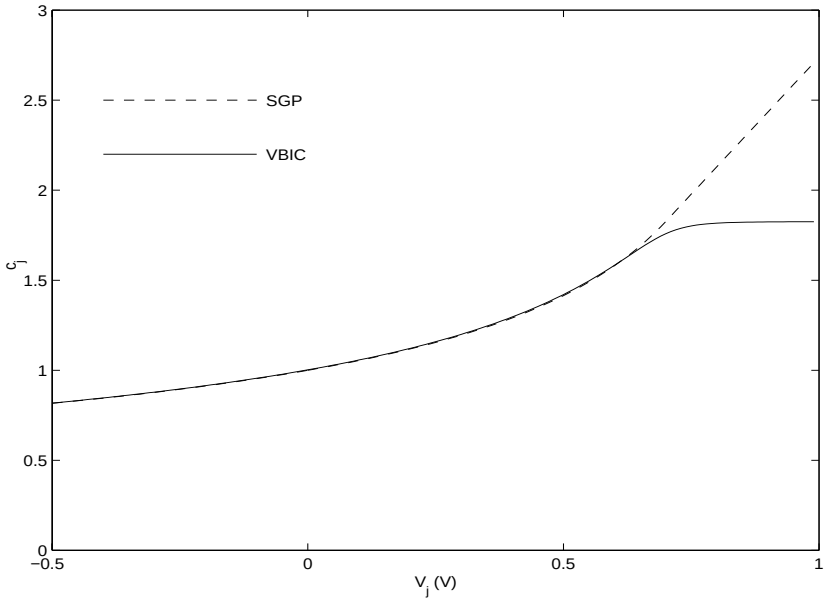

Figure 5 C_∞ continuous normalized depletion capacitance model.

The Early voltage components model the variation in q_b caused by changes in the depletion regions at the base-emitter and base-collector junctions, and the knee current components model the effects of high level injection. In this analysis the high level injection is considered to be in the base, whereas in normal NPNs it occurs when the base pushes out into the more lightly doped collector. This is handled in VBIC with the quasi-saturation model detailed below.

If the excess phase delay T_D is set to zero then I_{txf} in Figure 3 is just the I_{tzf} of equation (9). If $T_D > 0$ then the capacitance and inductance of the excess phase network of Figure 3 are set to T_D and $T_D/3$ respectively, and in the s domain the transfer function of the excess phase network is

$$V(xf2) = \frac{3I_{tzf}/T_D^2}{s^2 + 3s/T_D + 3/T_D^2} \tag{21}$$

which implements a second order polynomial approximation to ideal excess phase (Weil, 1978). The voltage on node `xf2` is then directly used as I_{txf}. This implementation of excess phase is consistent between small signal and transient analyses in a circuit simulator, and is independent of the numerical algorithms within a simulator. This is an advantage over an ideal excess phase model, as used in some simulators, which can only be implemented for small signal analysis. This leads to inconsistencies between small signal and transient simulations. Further, the implementation of a direct form of equation (21) in a circuit simulator depends on the numerical integration algorithms employed (Weil, 1978), whereas the equivalent network approach does not. Note that although the excess phase network in Figure 3 looks like it introduces 3 extra unknowns (2 node voltages and the inductor current) into the modified nodal formulation commonly used within circuit simulators, it can actually be implemented with only 2 additional simulation variables, by taking advantage of the observation that the voltage at node `xf2` is

equivalent to the current in the inductor.

The intrinsic charges are

$$Q_{be} = C_{JE} W_{BE} q_{je} + \tau_F I_{tzf} \tag{22}$$

where C_{JE} is the zero bias base-emitter depletion capacitance, W_{BE} is the partitioning of the base-emitter depletion capacitance between intrinsic and extrinsic components, q_{je} is defined in equation (19). τ_F is the forward transit time, modeled as

$$\tau_F = T_F(1 + Q_{TF} q_1)\left(1 + X_{TF} \exp\left(\frac{V_{bci}}{1.44 V_{TF}}\right)\left(\frac{q_b I_{tzf}}{q_b I_{tzf} + I_{TF}}\right)^2\right) \tag{23}$$

which is the SGP model, with an additional term in q_1 added to model the change in base transit time as the base-emitter and base-collector depletion region edges move with bias. The extrinsic base-emitter charge is

$$Q_{bex} = C_{JE}(1 - W_{BE}) q_j(V_{bex}, P_E, M_E, F_C, A_{JE}) \tag{24}$$

where it is apparent that $0 \le W_{BE} \le 1$ should hold, and V_{bex} is the extrinsic base-emitter bias, between nodes `bx` and `ei` in Figure 3.

The intrinsic base-collector charge is

$$Q_{bc} = C_{JC} q_{jc} + T_R q_b I_{tzr} + Q_{CO} K_{bci} \tag{25}$$

where C_{JC} is the zero bias base-collector depletion capacitance, q_{jc} is defined in equation (19), and T_R is the reverse transit time. The term $Q_{CO} K_{bci}$ models the diffusion charge associated with base pushout into the collector, and it and a similar extrinsic term

$$Q_{bcx} = Q_{CO} K_{bcx} \tag{26}$$

will be addressed below.

The base charge appears in both the transport current model, via the normalized base charge, and explicitly in the charge elements. By comparing the equivalent terms it is apparent that

$$C_{JE} V_{ER} = C_{JC} V_{EF} (A_e / A_c) = T_F I_{KF} = T_R I_{KR} = \int_0^w p \, dx = Q_{b0} \tag{27}$$

should be true for the transport and charge models to be consistent (where the second term includes only the portion of C_{JC} under the emitter, because the analyses are for the 1 dimensional intrinsic transistor). The relations (27) are not enforced in VBIC, both for compatibility with SGP, and to allow more degrees of freedom in fitting measured device characteristics. However, these relations are important for building process and geometry level models on top of VBIC, which are required for accurate statistical BJT modeling (McAndrew, 1997).

The major difference between the above transport current formulation of VBIC and that of SGP is the Early effect modeling via the q_1 term. In SGP this is approximated by (Nagel, 1975)

$$q_1 = \frac{1}{1 - \frac{V_{bei}}{V_{AR}} - \frac{V_{bci}}{V_{AF}}}. \tag{28}$$

Equation (28) cannot model the bias dependence of output conductance well over a wide range of biases, because it has linearized the dependence of depletion charge on applied bias. Figure 6 compares I_e/g_o^r modeling of VBIC and SGP. SGP cannot even qualitatively model the observed trends in measured data, it has the linear variation of equation (28), whereas VBIC models the onset of a fully depleted base region well. Therefore for improved accuracy of modeling, backward compatibility of VBIC to SGP for the Early effect modeling was not maintained.

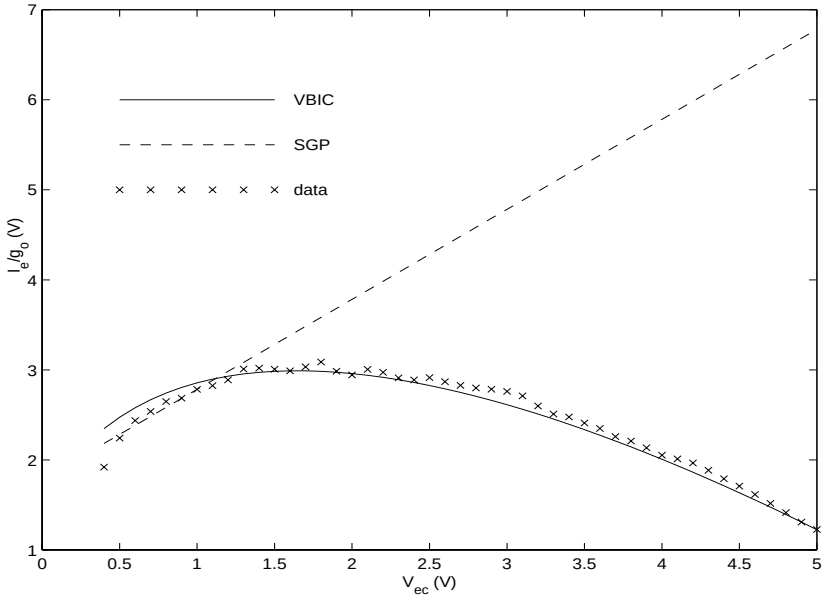

Figure 6 Early effect modeling of VBIC and SGP.

The base current elements of VBIC model recombination and generation currents. Three mechanisms are important, Shockley-Read-Hall recombination,

$$R_{srh} = \frac{np - n_{ie}^2}{\tau_h(n + n_{ie}) + \tau_e(p + n_{ie})}, \tag{29}$$

where τ_e and τ_h are the electron and hole trapping lifetimes, respectively, Auger recombination,

$$R_{aug} = (c_e n + c_h p)(np - n_{ie}^2), \tag{30}$$

where c_e and c_h are the Auger rate constants for electrons and holes, respectively, and surface hole recombination, modeled as a recombination current density

$$J_{hec} = qS_h(p_{ec} - p_{ec0}) \tag{31}$$

where S_h is the hole surface recombination velocity at the emitter, p_{ec} is the hole concentration at the emitter contact, and p_{ec0} is the equilibrium value for p_{ec}. All analyses below are for situations well out of equilibrium, so $np \gg n_{ie}^2$.

For a shallow emitter, equating the surface recombination current density for holes to the hole diffusion current from the edge of the base gives

$$qS_h p_{ec} \approx qV_{tv}\mu_h \frac{\partial p}{\partial x} \approx qV_{tv}\mu_h \frac{n_{ie}^2 \exp(V_{bei}/V_{tv})/N_d - p_{ec}}{w_e} \tag{32}$$

where μ_h is the hole mobility, N_d is the doping density in the emitter (so the equilibrium hole concentration is nearly n_{ie}^2/N_d), and w_e is the depth of the emitter. This gives

$$p_{ec} \approx \frac{n_{ie}^2 \exp(V_{bei}/V_{tv})}{N_d(1 + S_h w_e/(V_{tv}\mu_h))} \tag{33}$$

and thus the surface recombination current is close to proportional to $\exp(V_{bei}/V_{tv})$.

For recombination in the quasi neutral emitter $n \approx N_d \gg p$, and $np \gg n_{ie}^2$, therefore

$$R_{srh} \approx \frac{p}{\tau_h}, R_{aug} \approx c_e n^2 p \tag{34}$$

and because p is proportional to $\exp(V_{bei}/V_{tv})$ the quasi neutral region recombination current is also close to proportional to $\exp(V_{bei}/V_{tv})$.

In the base-emitter space charge region there is little Auger recombination (this process involves 3 interacting mobile carriers and is only likely in regions of high carrier concentrations), so Shockley-Read-Hall recombination dominates. $\phi_e \approx 0$ and $\phi_h \approx V_{bei}$ in this region, so from equations (3), (4), and (29),

$$R_{srh} \approx \frac{n_{ie}\exp(V_{bei}/V_{tv})}{\tau_h(\exp(\psi/V_{tv}) + 1) + \tau_e(\exp((V_{bei} - \psi)/V_{tv}) + 1)}. \tag{35}$$

This rate is maximized for

$$\psi = \frac{V_{bei} - V_{tv}\log(\tau_h/\tau_e)}{2} \tag{36}$$

and for $\tau_h \approx \tau_e$ has a value

$$R_{srh} \approx \frac{n_{ie}\exp(V_{bei}/(2V_{tv}))}{\tau_h + \tau_e}. \tag{37}$$

The space charge recombination current is therefore close to proportional to $\exp(V_{bei}/(2V_{tv}))$. Based on the above physical analyses, the base-emitter component of the intrinsic transistor base current in VBIC is modeled as

$$I_{be} = W_{BE}\left(I_{BEI}\left(\exp\left(\frac{V_{bei}}{N_{EI}V_{tv}}\right)-1\right)+I_{BEN}\left(\exp\left(\frac{V_{bei}}{N_{EN}V_{tv}}\right)-1\right)\right) \tag{38}$$

which includes both an ideal component, modeled with a saturation current I_{BEI} and ideality factor $N_{EI}\approx 1$, that comprises the emitter contact and quasi neutral region recombination, and a nonideal component for the space charge region component, modeled with saturation current I_{BEN} and ideality factor $N_{EN}\approx 2$. The ideality factors are treated as model parameters, and can be quite different from the values of 1 or 2 for HBTs. The base-collector component is similarly modeled as

$$I_{bc} = I_{BCI}\left(\exp\left(\frac{V_{bci}}{N_{CI}V_{tv}}\right)-1\right)+I_{BCN}\left(\exp\left(\frac{V_{bci}}{N_{CN}V_{tv}}\right)-1\right). \tag{39}$$

The extrinsic base-emitter recombination current is

$$I_{bex} = (1-W_{BE})\left(I_{BEI}\left(\exp\left(\frac{V_{bex}}{N_{EI}V_{tv}}\right)-1\right)+I_{BEN}\left(\exp\left(\frac{V_{bex}}{N_{EN}V_{tv}}\right)-1\right)\right). \tag{40}$$

From the physical analyses above, it is clear that the collector current primarily depends on the base doping, and the base current depends primarily on recombination and generation in the emitter region. Consequently, very different physical mechanisms control the collector and base currents. Relating them via a phenomenological parameter such as B_F, which is done in the SGP model, is therefore undesirable, and causes problems for statistical BJT modeling (McAndrew, 1997). This is why VBIC explicitly separates the base and collector current modeling.

The weak avalanche current I_{gc} is (Kloosterman, 1988)

$$I_{gc} = (I_{tzf}-I_{tzr}-I_{bc})A_{VC1}V_{gci}\exp\left(-A_{VC2}V_{gci}^{M_C-1}\right) \tag{41}$$

where A_{VC1} and A_{VC2} are model parameters, and V_{gci} is $P_C - V_{bci}$ limited, in a C_∞ continuous manner, to be greater than 0.

The intrinsic base resistance R_{BI} is modulated by the normalized base charge q_b. This accounts both for the base width variation from the Early effect, and the decrease in resistivity from increased mobile carrier concentration under high level injection conditions. VBIC does not include the I_{RB} emitter crowding modulation model of SGP. This effect can be taken into account, to a first order, by using the parameter W_{BE} to partition some of the base-emitter component of base current to I_{bex}, which is "external" to R_{BI}. This does not work well over all biases, however a simple model of emitter crowding, consistent for both DC and AC modeling, has not yet been developed.

If the model is biased so that the base region becomes depleted of charge, the modulated base resistance R_{BI}/q_b can become very large. q_b is limited to a lower value of 10^{-4} in VBIC (in a C_∞ continuous manner), but this is still sufficiently small to allow the model to support an unrealistically high V_{be} during a transient simulation for a device coming out of having a depleted base region. Multidimensional effects cause the device to turn on in a distributed manner from

the edge of the emitter under such circumstances, and partitioning some of the base-emitter component of base current to I_{bex} prevents modeling the unrealistically high V_{be} values.

The parasitic transistor is modeled similarly to the intrinsic transistor.

$$I_{tfp} = I_{SP}\frac{W_{SP}\exp\left(\frac{V_{bep}}{N_{FP}V_{tv}}\right) + (1 - W_{SP})\exp\left(\frac{V_{bci}}{N_{FP}V_{tv}}\right) - 1}{q_{bp}} \tag{42}$$

$$I_{trp} = I_{SP}\frac{\exp(V_{bcp}/(N_{FP}V_{tv})) - 1}{q_{bp}} \tag{43}$$

where the parasitic normalized base charge includes only a forward high level injection component,

$$q_{bp} = 1 + \frac{I_{SP}\left(W_{SP}\exp\left(\frac{V_{bep}}{N_{FP}V_{tv}}\right) + (1 - W_{SP})\exp\left(\frac{V_{bci}}{N_{FP}V_{tv}}\right) - 1\right)}{q_{bp}I_{KP}}. \tag{44}$$

Here I_{SP}, N_{FP}, and I_{KP} are the saturation current, ideality factor, and knee current for the parasitic transistor. The biases V_{bep} and V_{bcp} are between nodes `bx` and `bp`, and `si` and `bp`, respectively. The partitioning factor W_{SP} can be used to select a base-emitter control bias for the parasitic transistor either from between nodes `bx` and `bp`, or from the base-collector of the intrinsic transistor, between nodes `bi` and `ci`, as Figure 3 shows. The structure of a particular transistor determines which is more appropriate.

Although VBIC does not include a complete Gummel-Poon transistor for the parasitic, it does model the most important aspects of the behavior of this device. The parasitic transport current, including high level injection, models the substrate current when the intrinsic transistor goes into saturation. This is not included in the SGP model, yet is critical for accurate modeling of BJT behavior in saturation.

The other elements of the parasitic transistor model are

$$I_{bep} = I_{BEIP}\left(\exp\left(\frac{V_{bep}}{N_{CI}V_{tv}}\right) - 1\right) + I_{BENP}\left(\exp\left(\frac{V_{bep}}{N_{CN}V_{tv}}\right) - 1\right), \tag{45}$$

$$I_{bcp} = I_{BCIP}\left(\exp\left(\frac{V_{bcp}}{N_{CIP}V_{tv}}\right) - 1\right) + I_{BCNP}\left(\exp\left(\frac{V_{bcp}}{N_{CNP}V_{tv}}\right) - 1\right), \tag{46}$$

$$Q_{bep} = C_{JEP}q_j(V_{bep}, P_C, M_C, F_C, A_{JC}) + T_R q_{bp} I_{tfp}, \tag{47}$$

and

$$Q_{bcp} = C_{JCP}q_j(V_{bcp}, P_S, M_S, F_C, A_{JS}). \tag{48}$$

The parasitic base-collector charge Q_{bcp} is important for modeling collector-substrate capacitance. And although it normally should be reverse biased, the parasitic base-collector base current component I_{bcp} is important for detecting any inadvertent forward biasing of the collector-substrate junction. The parasitic base-emitter components are nearly in parallel with the intrinsic base-collector components. This means that these elements could be modeled via I_{bc} and Q_{bc}, however the parasitic base-emitter elements are still useful for accurate modeling of the distributed nature of devices. The parasitic transistor modeling is completed with the modulated parasitic base resistance R_{BIP}/q_{bp}.

One of the major deficiencies of the SGP model is its lack of modeling of quasi-saturation, when the base pushes into, and modulates the conductivity of, the collector. The Kull-Nagel model (Kull, 1985) is the most widely accepted basis for quasi-saturation modeling. However, this model can exhibit a negative output conductance at high V_{be}, see Figure 7. VBIC modifies the Kull-Nagel model to avoid the negative output conductance problem, and includes an empirical model of the increase of collector current at high bias.

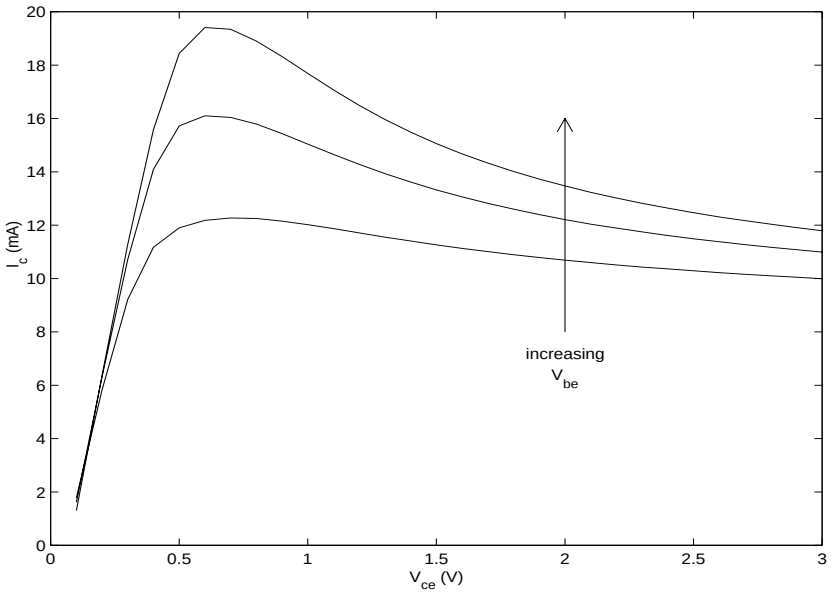

Figure 7 Negative output conductance from Kull-Nagel model.

Consider the lightly doped collector region between the base-collector junction x_{bc} and the highly doped buried layer x_{bl} in Figure 4. Integrating equation (2) across this region gives

$$J_{ex} = -\frac{q\mu_e}{x_{bl} - x_{bc}} \int_{\phi_{ec}}^{\phi_{ex}} n \, d\phi_e \tag{49}$$

where ϕ_{ex} is the electron quasi-Fermi potential at the buried layer. Quasi-neutrality in the lightly doped collector region, $n = p + N$ where N is the net doping level, gives

$$np = p(p + N) = n_{ie}^2 \exp\left(\frac{\phi_h - \phi_e}{V_{tv}}\right). \tag{50}$$

Differentiating and manipulating terms

$$(2p + N)\frac{\partial p}{\partial x} = -\frac{n_{ie}^2}{V_{tv}}\exp\left(\frac{\phi_h - \phi_e}{V_{tv}}\right)\frac{\partial \phi_e}{\partial x} = -\frac{np}{V_{tv}}\frac{\partial \phi_e}{\partial x} \tag{51}$$

and substituting equation (51) into equation (49) gives

$$J_{ex} = \frac{qV_{tv}\mu_e}{x_{bl} - x_{bc}}\int_{p_{bc}}^{p_{bl}}\left(2 + \frac{N}{p}\right)dp = \frac{qV_{tv}\mu_e}{x_{bl} - x_{bc}}\left(2(p_{bl} - p_{bc}) + N\log\left(\frac{p_{bl}}{p_{bc}}\right)\right) \tag{52}$$

where p_{bc} and p_{bl} are the mobile hole concentrations at $x = x_{bc}$ and $x = x_{bl}$, respectively. At the base-collector junction, equation (50) gives a mobile electron concentration

$$n_{bc} = \frac{N}{2}\left(1 + \sqrt{1 + \frac{4n_{ie}^2}{N^2}\exp\left(\frac{V_{bci}}{V_{tv}}\right)}\right) \tag{53}$$

and similarly at the buried layer

$$n_{bl} = \frac{N}{2}\left(1 + \sqrt{1 + \frac{4n_{ie}^2}{N^2}\exp\left(\frac{V_{bcx}}{V_{tv}}\right)}\right) \tag{54}$$

where V_{bcx} is the extrinsic base-collector bias, between nodes `bi` and `cx` of Figure 3. Therefore

$$p_{bl} - p_{bc} = n_{bl} - n_{bc} = \frac{N}{2}\left(\sqrt{1 + \frac{4n_{ie}^2}{N^2}\exp\left(\frac{V_{bcx}}{V_{tv}}\right)} - \sqrt{1 + \frac{4n_{ie}^2}{N^2}\exp\left(\frac{V_{bci}}{V_{tv}}\right)}\right) \tag{55}$$

and

$$\frac{p_{bl}}{p_{bc}} = \frac{n_{bc}}{n_{bl}}\exp\left(\frac{V_{bcx} - V_{bci}}{V_{tv}}\right) = \frac{1 + \sqrt{1 + \frac{4n_{ie}^2}{N^2}\exp\left(\frac{V_{bci}}{V_{tv}}\right)}}{1 + \sqrt{1 + \frac{4n_{ie}^2}{N^2}\exp\left(\frac{V_{bcx}}{V_{tv}}\right)}}\exp\left(\frac{V_{bcx} - V_{bci}}{V_{tv}}\right). \tag{56}$$

Substituting equations (55) and (56) into equation (52) gives the Kull-Nagel quasi-saturation model (without velocity saturation) for the lightly doped collector

$$I_{epi0} = \frac{V_{rci} + V_{tv}\left(K_{bci} - K_{bcx} - \log\left(\frac{K_{bci}+1}{K_{bcx}+1}\right)\right)}{R_{CI}} \tag{57}$$

$$K_{bci} = \sqrt{1 + G_{AMM}\exp\left(\frac{V_{bci}}{V_{tv}}\right)}, K_{bcx} = \sqrt{1 + G_{AMM}\exp\left(\frac{V_{bcx}}{V_{tv}}\right)} \tag{58}$$

where $V_{rci} = V_{bci} - V_{bcx}$ is the bias across the intrinsic collector resistance $R_{CI} = (x_{bl} - x_{bc})/(qAN\mu_e)$ (A being the area), and $G_{AMM} = (2n_{ie}/N)^2$ is the collector doping factor parameter. VBIC models the current in the modulated resistor R_{CI} as

$$I_{rci} = \frac{I_{epi0}}{\sqrt{1 + \left(\frac{R_{CI}I_{epi0}/V_O}{1 + \sqrt{0.01 + V_{rci}^2}/(2V_O H_{RCF})}\right)^2}}. \tag{59}$$

This accounts for velocity saturation modeled as $\mu_e = \mu_{e0}/\sqrt{1 + (\mu_{e0}\nabla\phi_e/v_{sat})^2}$ rather than the original formulation (Kull, 1985) $\mu_e = \mu_{e0}/(1 + \mu_{e0}|\nabla\phi_e|/v_{sat})$, and so avoids the discontinuity in derivative of the absolute value function. The formulation used in VBIC also avoids the negative output conductance apparent in Figure 7, and empirically models the increase in collector with increased V_{rci} at high V_{bci} via the H_{RCF} term.

The temperature mappings of the VBIC parameters are as follows. All resistance temperature variations are modeled with the empirical mobility temperature relation (Jacoboni, 1977)

$$R(T) = R(T_{nom})\left(\frac{T}{T_{nom}}\right)^{X_R} \tag{60}$$

with separate exponents X_R for each of the emitter, base, collector, and substrate. The temperatures here are all in degrees Kelvin. The saturation currents vary with temperature as, for example for I_S,

$$I_S(T) = I_S(T_{nom})\left(\left(\frac{T}{T_{nom}}\right)^{X_{IS}}\exp\left(-E_A\frac{1 - T/T_{nom}}{V_{tv}}\right)\right)^{1/N_F} \tag{61}$$

where there is a separate exponent X_{IS} and activation energy E_A for each saturation current. The built-in potential P and zero bias junction capacitance C_J parameters are modeled over temperature similarly to the SGP model, with a modification to avoid the built-in potential going negative for high temperatures (Booth, 1993),

$$P(T) = \Psi + \frac{2kT}{q}\ln\left(\frac{1 + \sqrt{1 + 4\exp(-q\Psi/kT)}}{2}\right), \tag{62}$$

$$\Psi = \frac{2kT}{q}\ln\left(\exp\left(\frac{qP(T_{nom})}{2kT_{nom}}\right) - \exp\left(-\frac{qP(T_{nom})}{2kT_{nom}}\right)\right) \quad , \tag{63}$$

$$-\frac{3kt}{q}\ln\left(\frac{T}{T_{nom}}\right) - E_A\left(\frac{T}{T_{nom}} - 1\right)$$

$$.C_J(T) = C_J(T_{nom})\left(\frac{P(T_{nom})}{P(T)}\right)^M . \tag{64}$$

N_F, N_R and A_{VC1} are modeled as having a linear temperature dependence. The collector doping parameter G_{AMM} is modeled over temperature as in equation (61), and the collector drift saturation voltage V_O is modeled over temperature as in equation (60) (Kull, 1985).

The electrothermal modeling in VBIC follows the formulation of Vogelsong (1989) and McAndrew (1992). All of the branch constituent relations detailed above are modified to include a dependence on the local temperature rise, the voltage at the node `dt`, as defined in the temperature mappings above. This greatly complicates the modeling equations, however the procedure for doing this is completely automated in VBIC, and is done using symbolic algebra software. The power dissipation I_{th} is

$$\begin{aligned} I_{th} = {} & I_{be}V_{bei} + I_{bex}V_{bex} + I_{bc}V_{bci} + (I_{tzf} - I_{tzr})(V_{bei} - V_{bci}) + I_{bep}V_{bep} \\ & + I_{bcp}V_{bcp} + (I_{tfp} - I_{trp})(V_{bep} - V_{bcp}) + I_{rcx}V_{rcx} + I_{rci}V_{rci} \\ & + I_{rbx}V_{rbx} + I_{rbi}V_{rbi} + I_{re}V_{re} + I_{rbp}V_{rbp} + I_{rs}V_{rs} - I_{gc}V_{bci} \end{aligned} \tag{65}$$

which is the sum of the products of branch currents and branch voltages over all elements of the VBIC equivalent network that do not store energy.

Note that in the VBIC implementation of electrothermal modeling, all of the branch constituent relations defined above become significantly more complex because of the implicit dependence on the local temperature node `dt`, through the model parameters which are functions of temperature. Although this results in a more complex model than if simple, first order effects were grafted on to the electrical model, it is the only way to guarantee modeling accuracy and consistency. The VBIC electrothermal code is automatically generated, with the temperature dependent parameter mappings being merged with the electrical branch constituent relations, and the derivatives being automatically generated via symbolic differentiation.

4 Parameter Extraction

Because of the similarity of some parts of VBIC to SGP, some parts of the parameter extraction strategy for VBIC are similar to those for SGP (Parker, 1995). However, the additional modeling features of VBIC require additional extraction algorithms, and because, unlike SGP, the DC and AC (capacitance) models are linked in VBIC through the Early effect model the extraction of the Early voltages requires the junction depletion capacitances to be modeled.

The first step in VBIC characterization (parameter determination) is therefore to extract the junction depletion capacitance parameters. This is easily done by using nonlinear least squares optimization to fit measured $C(V)$ data for each of the base-emitter, base-collector, and collector-substrate junctions. The base-collector capacitance is partitioned between C_{JC} and

C_{JEP} based on the relative geometries of the intrinsic (under the emitter) and extrinsic portions of the base-collector junction.

From forward output data at low V_{be_f} bias and reverse output data at low V_{bc} bias the output conductances normalized by current, g_o^f/I_c and g_o^r/I_e, are calculated, and then the solution of

$$\begin{bmatrix} q_{bcf} - c_{bcf}/(g_o^f/I_c) & q_{bef} \\ q_{bcr} & q_{ber} - c_{ber}/(g_o^r/I_e) \end{bmatrix} \begin{bmatrix} 1/V_{EF} \\ 1/V_{ER} \end{bmatrix} = \begin{bmatrix} -1 \\ -1 \end{bmatrix} \tag{66}$$

gives the VBIC Early voltages (McAndrew 1996). In equation (66) $q_{bef}(V_{be}^f, P_E, M_E)$ and $q_{bcf}(V_{bc}^f, P_C, M_C)$ the normalized base-emitter and base-collector depletion charges for the forward bias case, respectively, $q_{ber}(V_{be}^r, P_E, M_E)$ and $q_{bcr}(V_{bc}^r, P_C, M_C)$ are these charges for the reverse bias case, $c_{bcf} = \partial q_{bcf}/\partial V_{bc}^f$, and $c_{ber} = \partial q_{ber}/\partial V_{be}^r$.

The saturation currents and ideality factors for the various transport and recombination/ generation currents can be extracted in the usual manner from the slopes and intercepts of the variation of the logarithms of the currents as functions of the applied voltages. The data need to be filtered to exclude high level injection and resistive de-biasing effects. This is easily done by analyzing the derivative of the $\log(I)$ versus V data and excluding points that do not lie within some reasonable fraction, 5 to 10%, of its maximum value. The values obtained are then refined by optimization to fit the low bias data, both ideal and nonideal components. The activation energies for all saturation currents are determined by optimizing the fit to measured data, again filtered to keep only low biases, taken over temperature.

The knee currents can be determined as the current level at which the current gain drops to half its low bias value

Existing methods can be used to obtain initial values for the resistances. This can be difficult, and it is desirable to include both DC and AC data. Many of the simple procedures that have been proposed for BJT resistance calculation are based on oversimplifications of the model, and do not give realistic values. Optimization is used to refine the initial values, again preferably using DC and AC data. The quasi-saturation parameters are likewise obtained by optimization to output curves that show significant quasi-saturation effects. Other parameters, such as knee currents and Early voltages, should also be refined in this optimization.

The avalanche model parameters are optimized to fit the output conductance of data that is affected by avalanche.

Because VBIC has the same transit time model as SGP, the existing techniques for SGP transit time characterization are directly applicable to VBIC. However, the quasi-saturation model also affects high frequency modeling, via Q_{CO}, particularly where f_T falls rapidly with increasing I_c, so optimization is again used to fit the AC data.

Several techniques are available for characterizing the thermal resistance and capacitance. Physical calculation from layout can be used. However for R_{TH} if the electrical parameters are characterized at low bias and/or using pulsed measurements (Schaefer, 1996) then R_{TH} can be determined by optimizing the fit to high current data that shows significant self heating.

5 Relationship Between SGP and VBIC Parameters

Although VBIC offers many advantages over SGP, it was intended to default to being as close to SGP as possible. The Early effect model is the principle difference in formulation between

VBIC and SGP, the other features of VBIC are additions that, with the default parameters, are not active. Therefore, the easiest way to get started with VBIC is to use SGP as a base, and then incrementally include the features that are of greatest benefit for a given application. To help this Table 2 lists simple mappings from SGP parameters to VBIC parameters.

VBIC	Mapping	VBIC	Mapping	VBIC	Mapping
R_{CX}	R_C	M_C	M_{JC}	X_{TF}	X_{TF}
R_{CI}	0	C_{JCP}	C_{JS}	V_{TF}	V_{TF}
R_{BX}	R_{BM}	P_S	V_{JS}	I_{TF}	I_{TF}
R_{BI}	$R_B - R_{BM}$	M_S	M_{JS}	T_R	T_R
R_E	R_E	I_{BEI}	I_S/B_F	T_D	$\pi T_F P_{TF}/180$
I_S	I_S	N_{EI}	N_F	E_A	E_G
N_F	N_F	I_{BEN}	I_{SE}	E_{AIE}	E_G
N_R	N_R	N_{EN}	N_E	E_{AIC}	E_G
F_C	F_C	I_{BCI}	I_S/B_R	E_{ANE}	E_G
C_{JE}	C_{JE}	N_{CI}	N_R	E_{ANC}	E_G
P_E	V_{JE}	I_{BCN}	I_{SC}	X_{IS}	X_{TI}
M_E	M_{JE}	N_{CN}	N_C	X_{II}	$X_{TI} - X_{TB}$
C_{JC}	$C_{JC}X_{CJC}$	I_{KF}	I_{KF}	X_{IN}	$X_{TI} - X_{TB}$
C_{JEP}	$C_{JC}(1 - X_{CJC})$	I_{KR}	I_{KR}	K_{FN}	K_F
P_C	V_{JC}	T_F	T_F	A_{FN}	A_F

Table 2 Mappings from SGP to VBIC parameters

The Early voltages are the only parameters for which there is no direct mapping from SGP to VBIC. Because the Early effect models differ, the bias dependence of output conductance g_o cannot be matched between VBIC and SGP. Therefore the VBIC Early voltage parameters are derived from the SGP Early voltage parameters V_{AF} and V_{AR} by matching g_o^f/I_c and g_o^r/I_e between the two models at specific values of forward bias, V_{be}^f and V_{bc}^f, and reverse bias, V_{bc}^r and V_{be}^r (McAndrew, 1996). From the SGP model

$$\frac{g_o^f}{I_c} = \frac{1/V_{AF}}{1 - V_{be}^f/V_{AR} - V_{bc}^f/V_{AF}} \tag{67}$$

$$\frac{g_o^r}{I_e} = \frac{1/V_{AR}}{1 - V_{be}^r/V_{AR} - V_{bc}^r/V_{AF}} \tag{68}$$

are calculated, and then equation (66) is solved for V_{EF} and V_{ER}.

There is one other difference between the default parameters for VBIC and SGP. The F_C parameter, that limits how close to the built-in potential the junction voltage can go, for depletion charge and capacitance calculation, is 0.5 for SGP. This is too low and does not allow reasonable modeling of depletion capacitance into moderate forward bias. The VBIC default value is 0.9.

6 Conclusions

These notes have reviewed the VBIC model, and provided details of the equations used within VBIC. Examples of improved modeling aspects of VBIC have been given.
A VBIC distribution package is available electronically at

`http://www-sm.rz.fht-esslingen.de/institute/iafgp/neu/VBIC/index.html`

and this includes complete source code, a pseudo-code description of the model, test solvers, a program that maps SGP to VBIC model parameters, and other information related to VBIC.
VBIC is at present undergoing some minor changes, and the only major change that is being considered is an improved transit time model.

7 Acknowledgments

Many people have contributed to, and are continuing to contribute to, VBIC, including Jerry Seitchik, Derek Bowers, Didier Celi, Mark Dunn, Mark Foisy, Ian Getreu, Terry Magee, Marc McSwain, Shahriar Moinian, Kevin Negus, James Parker, David Roulston, Michael Schröter, Shaun Simpkins, Paul van Wijnen, and Larry Wagner.

8 References

Booth, R.V.H. (1993), private communication.

de Graaff, H. C. and Kloosterman, W. J. (1985) New formulation of the current and charge relations in bipolar transistors for modeling for CACD purposes. *IEEE Trans. ED*, **32**, 2415-9.

Getreu, I. E. (1976) Modeling the Bipolar Transistor. Tektronix, Beaverton.

Gummel, H. K., and Poon, H. C. (1970) An integral charge control model of bipolar transistors. *Bell Syst. Tech. J.*, **49**, 827-52.

Jacoboni, C., Canali, C., Ottaviani, G., and Alberigi Quaranta, A. (1977) A review of some charge transport properties of silicon. *Solid-State Electron.*, **20**, 77-89.

Jeong, H. and Fossum, J. G. (1989) A charge-based large-signal bipolar transistor model for device and circuit simulation. *IEEE Trans. ED*, **36**, 124-31.

Kloosterman, W. J. and de Graaff, H. C. (1988) Avalanche multiplication in a compact bipolar transistor model for circuit simulation. *Proc. IEEE BCTM*, 103-6.

Kull, G. M., Nagel, L. W., Lee, S.-W., Lloyd, P., Prendergast, E. J., and Dirks, H. K. (1985) A unified circuit model for bipolar transistors including quasi-saturation effects. *IEEE Trans. ED*, **32**, 1103-13.

McAndrew, C. C. (1992) A complete and consistent electrical/thermal HBT model. *Proc. IEEE BCTM*, 200-3.

McAndrew, C. C., Seitchik, J., Bowers, D., Dunn, M., Foisy, M., Getreu, I., Moinian, S., Parker, J., van Wijnen, P., and Wagner, L. (1995) VBIC95: an improved vertical, IC bipolar transistor model. *Proc. IEEE BCTM*, 170-7.

McAndrew, C. C., Seitchik, J., Bowers, D., Dunn, M., Foisy, M., Getreu, I., McSwain, M., Moinian, S., Parker, J., Roulston, D. J., Schroter, M., van Wijnen, P., and Wagner, L. (1996b) VBIC95: the vertical bipolar inter-company model. *IEEE JSSC*, **31**, 1476-83.

McAndrew, C. C. and Nagel, L. W. (1996) Early effect modeling in SPICE. *IEEE JSSC*, **31**, 136-8.

McAndrew, C. C., Bates, J., Ida, R. T., and Drennan, P. (1997) Efficient statistical BJT modeling, why β is more than I_c/I_b. *Proc. IEEE BCTM*.

Nagel, L. W. (1975) SPICE2: A computer program to simulate semiconductor circuits. Memo. no. ERL-520, Electronics Research Laboratory, University of California, Berkeley.

Parker, J. and Dunn, M. (1995) VBIC95 bipolar transistor model and associated parameter extraction. *HP EESof IC-CAP User's Meeting.*

Schaefer, B. and Dunn, M. (1996) Pulsed measurements and modeling for electro-thermal effect. *Proc. IEEE BCTM*, 110-7.

Stubing, H. and Rein, H.-M. (1987) A compact physical large-signal model for high-speed bipolar transistors at high current densities–Part I: one-dimensional model. *IEEE Trans. ED*, **34**, 1741-51.

Turgeon, L. J. and Mathews, J. R. (1980) A bipolar transistor model of quasi-saturation for use in computer-aided design (CAD). *Proc. IEEE IEDM*, 394-7.

Vogelsong, R. S. and Brzezinski, C. (1989) Simulation of thermal effects in electrical systems. *Proc. IEEE APEC*, 353-6.

Weil, P. B. and McNamee, L. P. (1978) Simulation of excess phase in bipolar transistors. *IEEE Trans. Circuits Syst.*, **2**, 114-6.